# Water adsorption on the stoichiometric and reduced $CeO_2(111)$ surface: a first-principles investigation

**Marco Fronzi,*[ab] Simone Piccinin,[a] Bernard Delley,[c] Enrico Traversa[b] and Catherine Stampfl[a]**

***Received 29th January 2009, Accepted 26th June 2009***
***First published as an Advance Article on the web 15th August 2009***
**DOI: 10.1039/b901831j**

We present a density functional theory investigation of the interaction between water and cerium oxide surfaces, considering both the stoichiometric and the reduced surfaces. We study the atomic structure and energetics of various configurations of water adsorption (for a water coverage of 0.25 ML) and account for the effect of temperature and pressure of the environment, containing both oxygen and water vapor, employing the *ab initio* atomistic thermodynamics approach. Through our investigation, we obtain the phase diagram of the water–ceria system, which enables us to discuss the stability of various surface structures as a function of the ambient conditions. For the stoichiometric surface, we find that the most stable configuration for water is when it is bonded at the cerium site, involving two O–H bonds of hydrogen and oxygen atoms at the surface. If oxygen vacancies are introduced at the surface, which is predicted under more reducing conditions, the binding energy of water is stronger, indicating an effective attractive interaction between water molecules and oxygen vacancies. Water dissociation, and the associated activation energies, are studied, and the role of oxygen vacancies is found to be crucial to stabilize the dissociated fragments. We present a detailed analysis of the stability of the water–ceria system as a function of the ambient conditions, and focus on two important surface processes: water adsorption/desorption on the stoichiometric surface and oxygen vacancy formation in the presence of water vapor. A study of the vibrational contribution to the free energy allows us to estimate the effect of this term on the stability range of adsorbed water.

## I. Introduction

Cerium oxide is an important and useful material for many technological applications. In particular, being a good ionic conductor[1,2] and, at the same time, having catalytically active surfaces,[3,4] it finds applications in sensors as well as fuel cell technologies.[3,5,6] In many catalyst applications, the relevant chemical processes taking place at the surfaces involve water, which can act as a spectator as well as a reactant.[7–9] For this reason, a detailed atomistic understanding of the interaction between water and ceria surfaces is of crucial importance. Recently, this topic has been investigated both theoretically and experimentally.[7,10–12] Experiments have shown that, depending on the temperature and pressure conditions, the presence of water can promote either the oxidation or the reduction of ceria surfaces.[13–15] This has been attributed to the different activity of different surface orientations.[10] It has been reported that water does not oxidize $Ce^{+3}$ sites (formed by oxygen vacancies) on the reduced $CeO_2(111)$ surface under ultra high vacuum (UHV) conditions at a temperature of 650 K.[10] Moreover, there is evidence of an increase in concentration of surface oxygen vacancies in the presence of water vapor.[10]

Several theoretical works have employed density functional theory (DFT) calculations to investigate the interaction of $H_2O$ with $CeO_2(111)$, both for the stoichiometric and the reduced surface (*i.e.* the surface containing oxygen vacancies).[7,11,12] Due to the different levels of theory adopted in these works, and to the different water coverages used in the simulations, there are various discrepancies of both quantitative and qualitative nature between these investigations.

Kumar *et al.*,[7] using DFT-GGA (generalized gradient approximation for the exchange and correlation energy) and a $(2 \times 1)$ surface unit cell, have investigated water adsorption and dissociation on both the clean and reduced surfaces. They find that water adsorbs preferentially on top of the cerium atom on the stoichiometric surface. The water binding energy is found to increase (more favorable) upon adsorption at an oxygen vacancy. Water dissociation, leading to oxidation of the surface and formation of $H_2$ in gas phase, is slightly energetically favorable when water is adsorbed on the reduced surface. In this work, the authors do not consider hydrogen adsorption on the surface, so, when water dissociation on the reduced surface is analyzed, they consider the reaction that leads to formation of $H_2$ in gas phase and the adsorption of an O atom on the surface at the vacancy site. In contrast, water dissociation is found to be less favorable when water is adsorbed on the clean surface. Watkins *et al.*,[11] using a combination of standard DFT-GGA and DFT-GGA + U, have investigated similar processes to Kumar *et al.* adopting

[a] *School of Physics, The University of Sydney, Sydney, New South Wales 2006, Australia. E-mail: marco@physics.usyd.edu.au*
[b] *University of Tor Vergata, Rome, Italy*
[c] *Paul-Scherrer-Institut, CH-5232 Villigen PSI, Switzerland*

 

what they call a $(2 \times \sqrt{2})$ surface unit cell. We assume, from geometric considerations, that this surface unit cell is what in our notation is labeled as a $(2 \times \sqrt{3})$ rect. surface cell. They find that on both the stoichiometric and reduced surfaces, water dissociation is energetically favorable. Their molecular dynamics simulations, performed only for the reduced surface, suggest that the activation barrier for the process is very small, which seems to contradict experimental evidence that finds water does not oxidize the reduced (111) surface.[10] Also, there seem to be significant discrepancies (both qualitative and quantitative) between these two theoretical works which can be partially attributed to the different water coverage studied, but that still await a detailed clarification. Also Chen *et al.*[12] employed DFT-GGA and DFT-GGA + U calculations to investigate water adsorption on the stoichiometric and reduced surface, using a $(1 \times \sqrt{3})$ rect. surface unit cell. In this case too, there are large quantitative differences in the calculated binding energies with the previous two works, most likely due to the different lateral interactions between the adsorbates induced by the different coverages simulated in the cited works. Clearly, a review of the above mentioned results and a rationalization of the discrepancies are necessary to achieve a consistent description of the water–ceria system.

In our previous work we studied the relative stability of a number of $CeO_2$ surfaces as a function of the chemical potential of oxygen.[16] We found the clean $CeO_2$(111) surface to be stable under oxygen-rich conditions, while the $CeO_2$(111) surface with oxygen vacancies is stable under more oxygen-poor conditions. A third termination, a "highly reduced" $CeO_2$(111) surface is found to be stable under extremely oxygen-poor conditions.[16] We also analyzed oxygen vacancy formation in the sub-surface region finding that this is more favorable (by 0.30 eV) than at the surface, in qualitative agreement with other recent *ab initio* studies.[17,18] A coexistence of surface and sub-surface oxygen vacancies is observed in a recent experimental work by Torbugge *et al.* using atomic-resolution dynamic force microscopy.[19]

Using standard DFT-GGA calculations, we examine the water–ceria system in a $(2 \times 2)$ surface unit cell, considering a large range of possible geometries to address water adsorption and dissociation on the stoichiometric, reduced and highly reduced surfaces. Comparing our results with the above-mentioned theoretical studies on the same system we are, first of all, able to give a comprehensive view of the involved processes and, to a certain degree, rationalize the discrepancies with and among previous works.

The relative stability of different surface structures is strongly influenced by the interaction with the environment, and in particular by the temperature and pressure of the surrounding gas phase in which the system operates. To account for these effects we employ first-principles atomistic thermodynamics, considering the system to be in thermodynamic equilibrium with an oxygen–water vapor atmosphere. This enables us to calculate the surface phase diagram of the water–ceria system as a function of pressure and temperature. Through the analysis of the portion of the phase diagram of relevance to realistic operating conditions, we are able to provide a theoretical understanding of the thermodynamics of the system. We validate our theoretical predictions by directly comparing our results with experimental data on two important surface processes: water desorption on the stoichiometric surface and water-induced formation of oxygen vacancies at the surface.

To complement this study, for the case where water dissociation is thermodynamically favorable, we analyze the activation barrier for this process by employing the linear synchronous transit method.[20] Kinetic considerations allow us to shed some light on the role played by water in stabilizing oxygen vacancies at the surface. For a particular case, we also investigate the role of the vibrational contributions to the free energy in the relative stability between different surface structures.

## II. Methodology

### A DFT-GGA calculations: comparison with other approaches, basis set and convergence

Cerium oxides ($CeO_{2-x}$, $0 < x < 1/2$) have been investigated extensively by means of DFT using a variety of approaches, ranging from plain DFT (LDA and GGA)[7,21] to DFT + U[22–25] and to hybrid functionals that include a portion of exact exchange.[17,26] These materials pose a great challenge to DFT methodologies due to the possibility of Ce changing oxidation state upon reduction. During this process, the excess electrons induced by the creation of oxygen vacancies can occupy the strongly-localized f orbitals. The local (LDA) or semilocal (GGA) approximations of the exchange and correlation potential, due to an incomplete cancellation of the Coulomb self-interaction, are considered unable to properly describe the electronic structure of these materials, especially in the presence of oxygen vacancies.

The inclusion of the Hubbard-U term in the DFT + U approach corrects the resulting electronic structure of the reduced ceria, favoring the insulating state with respect to the metallic solution. However, this approach suffers from a strong (linear) dependence of the energetics on the choice of the value of the parameter $U$ and on the choice of the localized projector functions that enter the definition of the U-dependent energy term.[23] For example, the DFT-GGA + U method using atomic orbitals as the localized projector functions, predicts that the reduction energy $\Delta H^{CeO_2 \rightarrow Ce_2O_3}$ can vary between $-5.1$ eV ($U = 0$ eV) and $-1.9$ eV ($U = 5.0$ eV), while the GGA-PBE value of $-4.18$ eV compares favorably with the experimental measurements ($-3.57$, $-4.03$ eV).[25] Typical values of $U$ for this system are in the range of 4.5–5.0 eV, obtained by empirically adjusting the $U$ term so as to reproduce the experimental spectroscopic features or by a self-consistent estimate based on the linear response method of Cococcioni and de Gironcoli.[27] These values of $U$ therefore give values of the reduction energy which are too low, and suggest that the empirical value of this parameter that would give a correct estimate of this quantity is of the order of 2 eV.[26] To avoid this undesirable dependence of the energetics on the parameter $U$, Fabris *et al.*[28] proposed using Wannier–Boys orbitals as the localized projector functions. This approach gives (almost) $U$-independent energetics, and a correct description of the electronic structure of the system. Nevertheless, the energetics of the system are in agreement with plain DFT.

When surfaces are considered, the surface energy of stoichiometric $CeO_2(111)$ is very similar when calculated with plain DFT and DFT + U and practically independent of the choice of U.[29] When surface vacancies are present, on the other hand, due to the reduction of some Ce ions from $Ce^{4+}$ to $Ce^{3+}$, standard DFT calculation are not able to describe the electron localization around Cerium atoms, giving a metallic solution for the system. The addition of the Hubbard-U term, forcing the system to have a semiconducting behavior, strongly alters the energetics of the system. For example, the oxygen vacancy formation energy on $CeO_2(111)$ changes between −2.15 eV and −4.95 eV upon a change of the projector functions using a value of U = 4.5 eV.[23] The plain DFT(GGA) value we compute in this work (−3.03 eV) is in between these two values, while the experimental value is in the range of −4.7 to −5.0 eV.[30] Part of this discrepancy (about 0.5 eV) can be attributed to the well known overestimate of plain DFT of the oxygen molecule binding energy. The energy difference between creating a surface and sub-surface vacancy (in the layer below) has been recently computed with both DFT + U and hybrid functionals by Gianduglia–Pirovano *et al.*,[17] showing that sub-surface vacancies are favored by 0.45 eV (hybrid functional), 0.47 eV (GGA + U) and 0.22 eV (LDA + U). As we have shown in our previous work,[16] the DFT-PBE result (0.30 eV) is in good agreement with these findings. Other works, employing standard DFT, calculate this energy difference finding the same qualitative trend: Kumar *et al.*, using a $(2 \times 1)$ surface unit cell, found this energy difference to be 0.12 eV, while Yang *et al.* obtained a value of 0.18 eV using a $(1 \times \sqrt{3})$ surface unit cell.[7,21]

Turning now to molecular adsorption on $CeO_2$ surfaces, Huang *et al.*[25] have shown how the energetics of CO physisorption on the (111) surface are equivalently described by plain DFT(GGA) and DFT-GGA + U. On the (110) surface, on the other hand, CO is strongly chemisorbed, leading to the reduction of two of the neighboring Ce ions. The binding energy obtained by employing DFT-GGA + U using atomic orbitals as projection functions again strongly depends on the choice of the parameter $U$. Using a standard value of $U$ = 4.5 eV, Huang *et al.* obtained an unrealistically large binding energy of 3.71 eV, while the experimental value is 2.12 eV. The experimental value is recovered using a much smaller value of $U$ (2 eV) than what is obtained through the self-consistent procedure or by adjusting the spectroscopic features to the experimental value. Plain DFT-GGA estimates this binding energy to be in the range of 1.5 to 1.9 eV,[25] in fair agreement with the experimental value.

Given the above discussion of some of the most recent reports on theoretical studies of cerium oxide surfaces, it is clear that, at present, no single approach gives a satisfactory description of both the electronic structure and the energetics of this system. It is also not clear whether the DFT + U method provides a systematic improvement of the energetics of this system compared to plain DFT. Also, as pointed out by Da Silva *et al.*, there is no unique $U$ that at the same time gives a reasonable description of structural parameters, relative energies of different oxides and spectroscopic properties.[26] Moreover, the large dependence of the energetics of the DFT + U approach on the choice of $U$ and projector functions is far from ideal. When such dependence is eliminated by a particular choice of projector functions (Wannier–Boys orbitals), one recovers the plain DFT energetics. In view of these considerations, in our study we adopt a plain DFT-GGA approach. The same choice has also been made by Yang *et al.* in their study of CO adsorption on $CeO_2$[21] and by Kumar *et al.* in their investigation of the interaction of water with the stoichiometric and reduced $CeO_2$ surfaces.[7] In the present paper, when a comparison is made between our calculations and previous works in which both DFT-GGA and DFT + U have been used, we always refer to the DFT-GGA values.

All calculations presented in this work are performed using the generalized gradient approximation for the exchange and correlation potential due to Perdew, Burke and Ernzerhof (PBE)[31] as implemented in the all-electron DMol$^3$ code. TheDMol$^3$ method employs fast-converging three-dimensional numerical integrations to calculate the matrix elements occurring in the Ritz variational method. The wave functions are expanded in terms of a double-numerical quality localized basis set with a real-space cutoff of 11 $a_0$. Polarization functions and scalar–relativistic corrections are incorporated explicitly. More details about the DMol$^3$ code can be found elsewhere.[32,33] We use $(2\times2)$ surface unit cells, and a vacuum region of $\approx$30 Å, which ensures negligible interaction between periodic replicas, and an $8 \times 8 \times 1$ $k$-point mesh, yielding 10 $k$-points in the irreducible part of the Brillouin Zone. Convergence tests for the number of atomic layers, number of $k$-points and real space cut-off show that our calculation setup yields well converged results for surface energies, as shown in our earlier publication, where the bulk properties of $CeO_2$ and $Ce_2O_3$ were also reported.[16]

We calculated the value of the counterpoise correction for the basis set superposition error (BSSE). We obtained this value for two configurations, water adsorbed on the clean surface and water adsorbed on the reduced surface, obtaining values of 0.050 and 0.039 eV, respectively, leading to an overestimation of the adsorption energy of less than 10%.

### B *Ab initio* atomistic thermodynamics

In order to analyze the thermodynamic stability of the considered surfaces, when exposed to a given environment, it is important to account for the effects of temperature and pressure of the surrounding atmosphere. This can be achieved by employing *ab initio* atomistic thermodynamics.[34] In this approach the system is considered to be in thermodynamic equilibrium with a gas phase environment, which is treated as a reservoir, therefore exchanging particles with the system without changing its chemical potential. The change in Gibbs free energy due to the formation of a structure, normalized by the unit area is:

$$\gamma(\{p_i\}, T) = \frac{1}{2A}\left[G - \sum_i N_i \mu_i(p_i, T)\right]. \qquad (1)$$

Here, $G$ is the Gibbs free energy of the solid with surface area $A$ (the factor $\frac{1}{2}$ is due to the presence of two identical surfaces, one on each side of the slab), $\mu_i(p_i,T)$ is the pressure- and temperature-dependent chemical potential of the various

 

species, $i$, present in the system, in this case $i$ = Ce, O and H. The term $N_i$ is the total number of atoms in component $i$ of the system.

In our system, the surface is in contact with an environment formed by a mixture of two different chemical species in the gas-phase, namely $O_2$ and $H_2O$. Considering first the case in which only oxygen is present, the range over which $\mu_O$ can be varied is not without bounds. If it becomes too low (oxygen-lean conditions) the oxide will decompose, while if it becomes too high (oxygen-rich conditions), oxygen will start condensing on the surface. How the oxygen-lean and -rich conditions can be determined quantitatively will be discussed in section IV.

To treat the case of a multi-component gas atmosphere we follow the approach of Sun *et al.*[35] Briefly, when two gas species are considered, depending on the gas phase reaction barriers, the equilibrium between the two components may or may not be reached. In our case, as we will see in the following sections, the range of allowed values for $\mu_O$ is such that, if the system is fully equilibrated, water is the dominant component.[36] Modeling this particular situation, the chemical potential of H atoms at the $CeO_2$ surface is therefore determined by an $H_2O$ reservoir. To make sure that water vapor remains the thermodynamically stable phase, the maximum value of $\mu_{H_2O}$ will be fixed at −0.91 eV, with respect to the total energy of the $H_2O$ molecule, which corresponds to the chemical potential of water at the experimental critical point.[35]

Once the above considerations are made, the chemical potential of hydrogen is determined by $\mu_O$ and $\mu_{H_2O}$, according to:

$$\mu_{H_2O}(p,T) = \mu_O(p,T) + 2\mu_H(p,T), \quad (2)$$

$$\mu_H(p,T) = \tfrac{1}{2}[\mu_{H_2O}(p,T) - 2\mu_O(p,T)]. \quad (3)$$

If the $CeO_2$ slab is thick enough to be considered as a reservoir, then we can approximate $CeO_2$ bulk to be in equilibrium with oxygen in the atmosphere, and we can consider the Ce chemical potential as being determined from the relation:

$$g_{CeO_2}(p,T) = 2\mu_O(p,T) + \mu_{Ce}(p,T), \quad (4)$$

where $g$ is the Gibbs free energy per unit formula. From these considerations, it is possible to rewrite eqn (1) as:

$$\gamma(\{p_i\},T) = \frac{1}{2A}[G^{Slab+Mol} - N_{Ce}g^{bulk}_{CeO_2}] + \frac{1}{2A}\left[\mu_{O_2}(p_O,T)\left(2N_{Ce} - N_O + \frac{N_H}{2}\right) - \mu_{H_2O}(p_{H_2O},T)\frac{N_H}{2}\right]. \quad (5)$$

The chemical potentials, $\mu_i(T,p)$, of oxygen and water vapor depend on temperature and pressure according to:[37]

$$\mu_O(p,T) = \frac{1}{2}\left[E_{O_2} + \tilde{\mu}_{O_2}(p^0,T) + k_B T \ln\left(\frac{p_{O_2}}{p^0}\right)\right], \quad (6)$$

$$\mu_{H_2O}(p,T) = E_{H_2O} + \tilde{\mu}_{H_2O}(p^0,T) + k_B T \ln\left(\frac{p_{H_2O}}{p^0}\right), \quad (7)$$

where $\tilde{\mu}_i(p^0,T)$ ($i$ = $O_2$, $H_2O$) is the chemical potential, including the vibrational and rotational contributions, at pressure $p^0$ = 1 atm, obtained from thermodynamic tables.[38] Eqn (6) and (7) give us an explicit analytic relation between chemical potentials and the temperature and pressure of the two gas reservoirs.

In the following we will measure the chemical potential of O and $H_2O$ with respect to the energy of the isolated molecules ($E_{O_2}$ and $E_{H_2O}$). We therefore define the relative chemical potential of oxygen to be $\Delta\mu_O(T,p) = \mu_O - \frac{1}{2}\mu_{O_2}$, and the relative chemical potential of water to be $\Delta\mu_{H_2O}(T,p) = \mu_{H_2O} - E_{H_2O}$.

If we assume that the vibrational and configurational contribution to the free energy, $G$, can be neglected, this allows us to identify the free energy, $G$, with the total energy, $E$, which can be computed directly through DFT calculations. Therefore, within this approach, the only variables that depend explicitly on $T$ and $p$ are the chemical potentials of oxygen and water. In section V, however, we present a detailed analysis of the vibrational contributions to the free energy for cases of special interest.

## III. Geometries and energetics

### A Adsorption of water

Using a (2 × 2) unit cell and a water coverage of 0.25 ML (*i.e.* one water molecule per unit cell on each side of the slab), we consider various configurations of the water molecule on the stoichiometric $CeO_2$(111) surface. In particular, we consider the adsorption site above the cerium atom, above the oxygen atom and between the cerium and the oxygen atoms at the surface. For each adsorption site, we consider different orientations of the hydrogen atoms, as depicted in Fig. 1.

The binding energy of an adsorbate on the surface is calculated as follows:

$$E_b = -[E_{Slab+Mol} - (E_{Slab} + E_{Mol})], \quad (8)$$

where $E_{Slab+Mol}$ and $E_{Slab}$ are the total energies of the slab–molecule system and the clean slab, respectively. $E_{Mol}$ is the energy of the adsorbate (in our case water, hydrogen, oxygen or hydroxyl) in the gas phase. In particular, for hydrogen and oxygen, we calculate the binding energy with respect to half the total energy of the diatomic molecule. For the case of adsorption on the clean unreconstructed surface, $E_{Slab}$ is the energy of the clean surface slab, while for adsorption on the reduced surface, $E_{Slab}$ is defined as the energy of the slab containing surface oxygen vacancies.

We start by calculating water adsorption on the clean $CeO_2$(111) surface. Table 1 gives the values of the binding energy for each configuration considered. It can be seen that the most favorable adsorption site (labeled Ce1 and shown in Fig. 1(a) and (b)) is the one above the cerium atom, with water having two $O_s$–H bonds, where each H atom is aligned close to a surface O atom (here $O_s$ indicates the closest oxygen atoms of the $CeO_2$(111) surface to the H atom). In this configuration, water is in a planar geometry, in agreement with experimental observations.[39,40] The binding energy for this configuration (0.49 eV) compares favorably with the experimental value

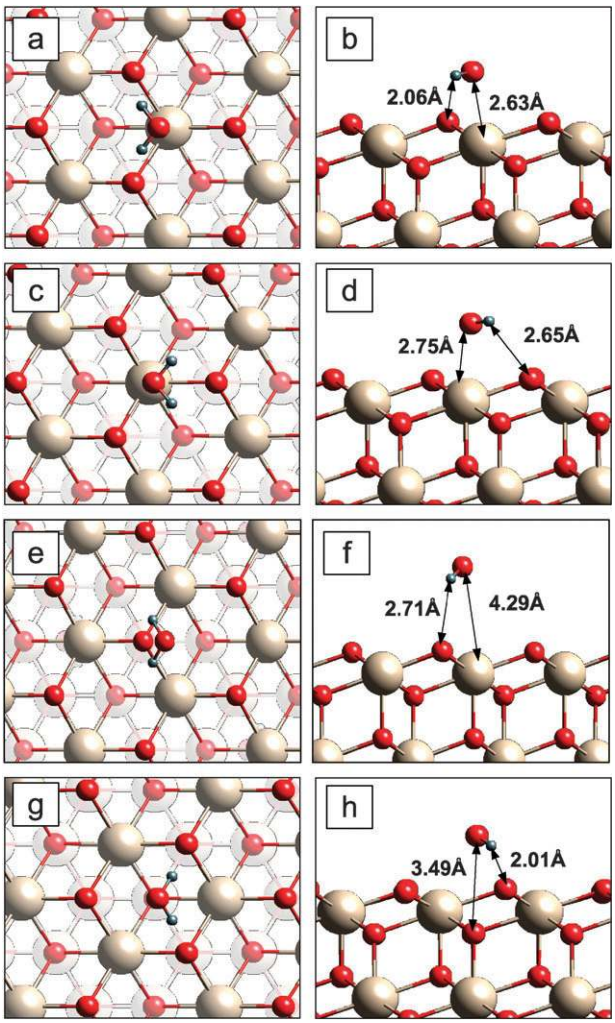


**Fig. 1** Top (left) and side (right) view of adsorption sites considered for a water molecule on $CeO_2$(111). Images (a) and (b) show $H_2O$ in the Ce1 configuration, (c) and (d) $H_2O$ in the Ce2 configuration, (e) and (f) in the O1, and (g) and (h) in the O2 configurations. Large gray and small red spheres indicate Ce and O atoms, respectively. The very small (gray) spheres represent H atoms. Selected inter-atomic distances are indicated.

**Table 1** Binding energies (in eV) of water on the $CeO_2$(111) surface in different configurations (see Fig. 1)

| | Binding energy/eV | |
|---|---|---|
| Adsorption site | This work | Other *ab initio* calculations |
| Ce1 | 0.49 | 0.51[a], 0.56[b] |
| Ce2 | 0.33 | 0.35[c] |
| O1 | 0.33 | — |
| O2 | 0.18 | — |

[a] Ref. 12. Using a $(1 \times \sqrt{3})$ rect. surface unit cell. [b] Ref. 7. Using a $(1 \times 2)$ surface unit cell [c] Ref. 11. Using a $(2 \times \sqrt{3})$ rect. surface unit cell.

(0.53 eV for a coverage of 0.2 ML[10] and 0.61 eV[41] (coverage not specified)), estimated from the analysis of temperature programmed desorption (TPD) experiments, as well as with other *ab initio* calculations (0.51 eV using a $(1 \times 2)$ surface unit cell[12] and 0.56 eV using a $(1 \times \sqrt{3})$ rect. surface unit cell[7]). We note that the value of the binding energy obtained by Watkins *et al.*[11] is somewhat smaller (0.35 eV) due to the different adsorption geometry considered in their work. The distance between the O atom in $H_2O$ and the closest Ce atom is 2.63 Å, which is 10% greater than the Ce–O distance in bulk $CeO_2$ (2.34 Å), while the $O_s$–H distance is 2.06 Å (see Fig. 1(b)). To analyze the nature of the interaction between the oxygen atom of $H_2O$ and the surface cerium atom, we studied the charge density difference induced by the adsorption of water on $CeO_2$(111), defined as the difference between the charge density of the adsorbate system and the sum of the isolated molecule slab (see Fig. 2(a)). This quantity does not suggest any net charge transfer between surface and water molecule, but shows a charge redistribution around both the Ce atom and the O atom of water, and a weak charge accumulation in the area between O and Ce.

Turning now to the reduced surfaces, which are favorable for low values of the oxygen chemical potential,[16] we consider three different configurations of water adsorbed at an oxygen vacancy in the $CeO_2$(111) surface. The geometries are shown in Fig. 3. In particular, the configuration with one H–$O_s$ bond (Fig. 3(a) and (b)) has a binding energy of 0.59 eV, while the configuration with two H–$O_s$ bonds (Fig. 3(c) and (d)) has a binding energy of 0.52 eV. A third configuration is also considered by decreasing the water molecule–vacancy distance and orienting the hydrogen atoms upwards (Fig. 3(e) and (f)). In this case we find a much larger binding energy of 1.28 eV. Therefore, when an oxygen vacancy is created on the surface, the binding energies are in general greater than on the clean, unreconstructed slab, indicating an effective attraction between the water molecule and the oxygen vacancies. To further investigate this, we show in Fig. 2 the induced charge density due to the adsorption of water on the reduced surface in the most favorable configuration. There is a clear redistribution of the electronic charge and an accumulation in the area between the oxygen atom of the water and the cerium atom face. Most likely, the increased binding energy is due to an enhanced electrostatic interaction induced by the presence of the oxygen vacancy.

Comparing our results with the previous works on this system, we find that our most stable configuration gives a

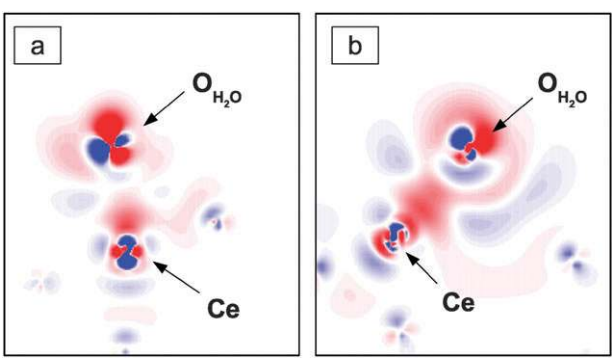


**Fig. 2** Induced charge density due to the adsorption of water on (a) the stoichiometric surface and (b) the reduced surface. The red areas indicate charge accumulation, while the blue areas indicate charge depletion.

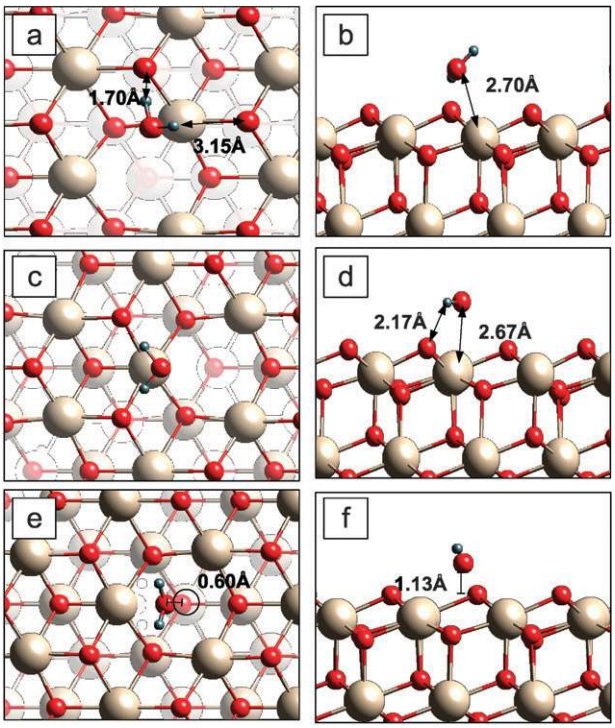


**Fig. 3** Top (left) and side (right) view of adsorption sites considered for a water molecule on the $CeO_2(111)$ surface with an oxygen vacancy, $CeO_2(111) + V_O$. Images (a) and (b) show $H_2O$ in the $V_O1$ configuration, (c) and (d) show $H_2O$ in the $V_O2$ configuration, and (e) and (f) show $H_2O$ in the $V_O3$ configuration. Large gray and small red spheres indicate Ce and O atoms, respectively. The very small (gray) spheres represent H atoms. Selected inter-atomic distances are indicated.

noticeably larger water binding energy than what has been found by Watkins *et al.*[11] (0.8 eV) and by Kumar *et al.* (0.72 eV). Possibly due to the small $(1 \times \sqrt{3})$ rect. unit cell adopted, Chen *et al.*[12] find that water does not bind to the reduced surface. However, in the absence of a detailed description of the adsorption geometry, it is difficult to directly compare these values of binding energy with our results.

To better understand the interaction between water and oxygen vacancies on $CeO_2(111)$ we consider the cost of creating an oxygen vacancy. Removing an oxygen atom from the first layer of a clean $CeO_2(111)$ slab in a $(2 \times 2)$ surface unit cell costs 3.03 eV, where the energy of the oxygen atom is measured with respect to half the total energy of an isolated oxygen molecule. On the other hand, if a water molecule is present on the surface, removing the nearest oxygen atom to the water molecule from the first layer costs 2.24 eV. In our previous work, we have calculated the cost of creating a sub-surface vacancy (in the layer below), when the surface not in contact with water. In a $(2 \times 2)$ surface unit cell, this value is 0.30 eV lower than the cost of creating a surface vacancy.[16] In contrast to surface vacancies, the cost of creating a sub-surface vacancy is only slightly affected by the presence of a water molecule adsorbed on the surface ($\sim$0.01 eV).

In light of these results we can conclude that, while sub-surface vacancies are more favorable in the absence of the water, in the presence of water, surface vacancies are more favorable. Also, given the significant reduction of the cost to create a vacancy in the first layer induced by the presence of water, we can predict that in a humid environment there will be an increase in the number of surface vacancies with respect to the case in which the surface is in vacuum. This is consistent with experimental findings that report that the presence of water increases the number of surface vacancies on $CeO_2(111)$.[10] In section IV we will further analyze the vacancy formation process including the effects of temperature and pressure of the gas reservoirs in contact with the surface.

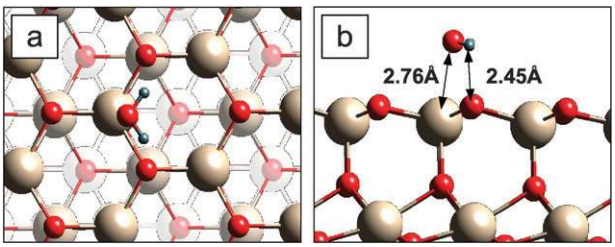


**Fig. 4** Top (left) and side (right) view of the adsorption site considered for a water molecule on the "highly reduced" Ce-terminated $CeO_2(111)$ surface, $CeO_2(111)$:Ce. Note that, due to the significant atomic relaxation, the O atoms become the uppermost species.[16] Large gray and small (red) spheres indicate Ce and O atoms, respectively. The very small (gray) spheres represent H atoms. Selected inter-atomic distances are indicated.

**Table 2** Binding energies of a H atom (in the Ce and O sites) and OH (in the Ce site) on the stoichiometric $CeO_2(111)$ surface and on the highly-reduced surface $CeO_2(111)$:Ce in the $(2 \times 2)$ surface unit cell, with respect to OH and (half) $H_2$ in the gas phase

| | Binding energy/eV | |
|---|---|---|
| Configuration | This work | Other *ab initio* calculations |
| H (in O) | 0.65 | 0.18[a] |
| H (in Ce) | −2.85 | — |
| OH | 1.11 | — |
| $CeO_2(111)$:Ce + H | −0.64 | — |
| $CeO_2(111)$:Ce + OH | 3.72 | — |

[a] Ref. 12. Using a $(2 \times \sqrt{3})$ rect. surface unit cell.

We now consider the adsorption of water on a highly-reduced ceria surface, favorable under extremely oxygen-poor conditions.[16] The surface structure resembles that of $Ce_2O_3(0001)$, and is characterized by the absence of the sub-surface oxygen layer. Fig. 4 shows the geometry of this configuration, which we label $CeO_2(111)$:Ce (as in our earlier publication, ref. 16), and the binding energies are given in Table 2. In this case, we have two O–H bonds with a distance of 2.45 Å between the hydrogen and oxygen atoms at the surface. The distance between the O atom in $H_2O$ and the surface Ce atom is 2.76 Å. The vertical distance between the molecule and the surface is 25% greater than for the case of the stoichiometric surface, and, correspondingly, the binding energy is lower: 0.31 eV in this case, compared to 0.49 eV on the stoichiometric surface.

### B Dissociation of water

After elucidating the adsorption process, we now turn to the dissociation of a water molecule on ceria, considering both the stoichiometric and the reduced surfaces (*i.e.* with oxygen

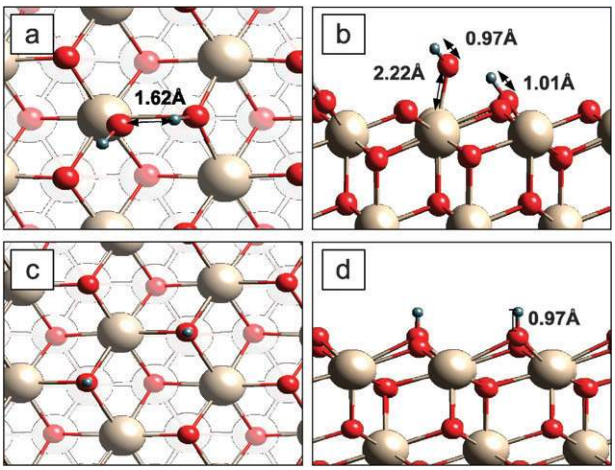


**Fig. 5** Top (left) and side (right) view of a dissociated water molecule on $CeO_2(111)$ [(a) and (b)] and on $CeO_2(111) + V_O$ [(c) and (d)]. Large gray and small (red) spheres indicate Ce and O atoms, respectively. The very small (gray) spheres represent H atoms. Selected inter-atomic distances are indicated.

vacancies). Watkins *et al.*[11] have investigated this process, addressing whether it is energetically favorable for the molecule to split and dissociatively adsorb, and what the most favorable configurations for the H and OH fragments are. For the case of the clean surface, it has been suggested that the water molecule dissociates into an OH group bonded to cerium and an H atom bonded to a surface oxygen atom. Relative to water adsorbed on the clean surface, this dissociated state is found to be 0.30 eV more stable.[11] For the case of the reduced surface, the same authors found water to dissociate into an OH group, which fills the oxygen vacancy and an H atom which bonds to a surface oxygen atom, with a total binding energy of 2.17 eV with respect to the water in gas phase. When comparing this dissociated state with water chemisorbed on an oxygen vacancy (0.80 eV), we infer that water dissociation is favored by 1.37 eV.

On the other hand, in our calculations, we find that the clean $CeO_2(111)$ surface does *not* dissociate water: the configuration with water physisorbed on the surface is favored by 0.13 eV with respect to the dissociated configuration (see Fig. 5(a) and (b)). We attribute part of the discrepancy with the results of ref. 11 to the fact that we consider a physisorbed configuration of water adsorbed on the clean surface that those authors did not investigate, which is energetically more favorable by 0.16 eV. When considering the same physisorbed configuration as ref. 11 (shown in Fig. 1(c) and (d)) we find a binding energy of 0.33 eV (obtained using a $(2 \times 2)$ surface unit cell) which compares very well with their published result (0.35 eV obtained with a $(2 \times \sqrt{3})$rect. surface unit cell).[11] As mentioned above, we, in addition, considered the configuration in which water has two $O_s$–H bonds, as shown in Fig. 1(a) and (b), which is 0.16 eV more stable. This result is in good agreement with the binding energy found in ref. 7, where the same configuration was considered. The additional discrepancy in dissociation energy is possibly due to the effect of lateral interactions between isolated hydrogen atoms belonging to different cells, as we will show later.

For the case of the reduced surface we find, in contrast to the clean surface, that the process of water dissociation is energetically favorable. A non-dissociated molecule binds to the oxygen vacancy, as shown in Fig. 3(e) and (f), with a binding energy of 1.28 eV. For the dissociated molecule, the OH fragment binds to the vacancy with the oxygen filling the vacancy site, while the H atom is bonded to a surface oxygen, in agreement with ref. 11. This configuration is shown in Fig. 5(c) and (d). The binding energy in this case is −1.40 eV with respect to water in gas phase. Water dissociation is therefore favored by 0.12 eV with respect to the non-dissociated state on the reduced surface, notably less than the value (1.37 eV) found in ref. 11. This qualitative difference between the clean and the reduced ceria surfaces stresses the importance of vacancies for water dissociation in this system.

As mentioned above, there is a large discrepancy between our value of dissociation energy on the reduced surface (0.12 eV) and the value computed by Watkins *et al.*,[11] which we infer to be 1.37 eV. This difference can be attributed, partly, to the different value of binding energy for water on the reduced surface (0.8 eV, compared to our value of 1.28 eV), possibly due to a different (less stable) adsorption geometry adopted in ref. 11. Also, the different choice of unit cell could play a significant role, since it might affect the lateral interactions between the adsorbates belonging to different unit cells. To quantify this effect, we perform a study of the dependence of the hydrogen atom binding energy on the surface unit cell geometry. Considering one adsorbate per unit cell, we find that in a $(2 \times 2)$ surface unit cell the hydrogen binding energy is 0.65 eV, while in a $(1 \times 1)$ cell it decreases to 0.21 eV, due to the electrostatic repulsion between the partially positively charged H adsorbates. This change therefore suggests that the coverage and the unit cell adopted in the study of water dissociation on ceria affects the energetics of the system, and might account for part of the discrepancies between calculations reported in the literature carried out at different coverages or adopting different unit cells.

On the other hand, we find that the water binding energy does not depend strongly on the coverage within the 0.25–0.50 ML range. This conclusion stems from the comparison of water binding energies obtained by using different surface unit cells. When we use a $(2 \times 1)$ surface unit cell, we find a water binding energy of 0.50 eV, while the value obtained using a $(2 \times 2)$ unit cell is 0.49 eV. This qualitatively different behavior compared with the case of hydrogen adsorption can be attributed to the different nature of the water–ceria interaction compared to the hydrogen–ceria one: weak physisorption in the first case, chemisorption in the second.

To rule out any effect of spin polarization, we also performed a spin-polarized calculations for selected systems where this contribution might be thought to be non negligible. Considering the $CeO_2(111)$ surface with oxygen vacancies, and $CeO_2(111)$ with water dissociated, we find the change in the surface energy to be less than 0.01 eV $Å^{-1}$. We therefore conclude that the spin polarization has a negligible effect in the energetics of our system, in agreement with ref. 21.

Having identified the dissociated structures, we now estimate the activation barrier for the dissociation reaction over the reduced surface. This is accomplished by locating the

 

transition state using the linear synchronous transit (LST) method. Further details about this method, including examples of its application, can be found in ref. 20. In the initial state for the dissociation reaction, the water molecule is adsorbed directly above the oxygen vacancy (Fig. 3(e) and (f)), while in the final state, the OH fragment is adsorbed in the oxygen vacancy, and the H atom is adsorbed atop a neighboring surface oxygen (Fig. 5(c) and (d)). The final configuration of the dissociation reaction therefore corresponds to the clean surface with two hydrogen atoms bonded on neighboring surface oxygen atoms. Fig. 6 shows the resulting energy diagram, *i.e.* the relative energies of the initial, final and transition states, and the corresponding geometries are illustrated. The gain in energy for water dissociation is 0.12 eV and the activation barrier is 2.35 eV. At the transition state the distances between the dissociating H atom and the oxygen atom of the water molecule and the surface oxygen (adsorption site) are 2.13 and 2.39 Å, respectively, while the distance between the dissociated H atom and the nearest cerium atom is 2.99 Å. Given the exponential dependence of the reaction rate on the activation energy, this process, having a barrier in excess of 2 eV, is extremely unlikely except at very high temperature. From this analysis we find that surface oxygen vacancies can act as centers of water dissociation since the dissociation is exothermic, although the high value of the activation barrier suggests that this process is an extremely rare event and, therefore, water molecules do not act as an oxidant for the reduced surface. The high kinetic barrier for water to oxidize the reduced surface and the small energy difference (0.12 eV) between water chemisorbed on a vacancy and water dissociated as to oxidize the surface could provide a rationale for the experimental evidence that water does not oxidize the reduced surface.[10] This point will be further elaborated on in the next section, where we present the phase diagram of the water–ceria system. We note here that Watkins *et al.*,[11] using molecular dynamics simulations, found that, at variance with our results, water readily dissociates on the reduced surface, which seems to contradict the experimental evidence.[10]

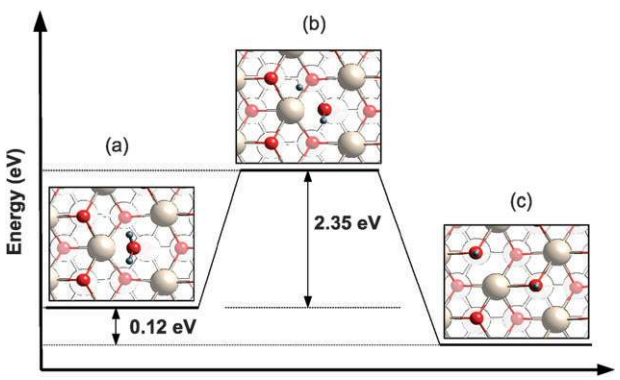


**Fig. 6** Schematic representation of water dissociation on the $CeO_2(111) + V_O$ surface showing relative energies and the activation barrier. Geometries of the reactant ($H_2O$) (a), product (c) and transition state (b), are shown. Large gray and small (red) spheres indicate Ce and O atoms, respectively. The very small (gray) spheres represent H atoms.

## IV. Energetics and thermodynamics

Having identified the relevant structures for the ceria–water system, we can now study the stability of each surface when in contact with a gas reservoir. In particular, we are interested in an atmosphere where both $O_2$ and $H_2O$ are present. The key quantity of this study is the surface free energy (eqn (5)) as function of the chemical potential of O and $H_2O$. We can then identify the structures that minimize the surface free energy for a particular value of $\mu_O$ and $\mu_{H_2O}$, and which, therefore, are the most stable.

The oxygen-lean and oxygen-rich conditions can be found considering oxygen to be in thermal equilibrium with bulk $CeO_2$:

$$2\mu_O + \mu_{Ce} = g^{bulk}_{CeO_2}. \quad (9)$$

Under oxygen-lean conditions, $CeO_2$ will start decomposing into Ce metal and $O_2$ gas. The atomic chemical potential of cerium in this situation is taken to be that of a cerium atom in bulk Ce, which is the upper limit:

$$[\mu_{Ce}]_{max} = g^{bulk}_{Ce}. \quad (10)$$

Using eqn (9), the value of $\mu_O$ under oxygen-poor conditions is:

$$[\mu_O]_{min} = \frac{1}{2}[g^{bulk}_{CeO_2} - g^{bulk}_{Ce}]. \quad (11)$$

We take $g^{bulk}_{CeO_2}$ and $g^{bulk}_{Ce}$ as the temperature $T = 0$, and pressure $p = 0$, total energies of the respective systems from DFT calculations.

The oxygen-rich limit corresponds to oxygen molecules condensing on the surface. Hence, we assume the oxygen chemical potential under oxygen-rich conditions to be:

$$[\mu_O]_{max} = \tfrac{1}{2}E_{O_2}. \quad (12)$$

Defining $\Delta\mu_O = \mu_O - \frac{1}{2}E_{O_2}$, the range of allowed values for $\Delta\mu_O$ is:

$$\frac{1}{2}(g^{bulk}_{CeO_2} - g^{bulk}_{Ce} - E_{O_2}) \le \Delta\mu_O \le 0. \quad (13)$$

Using the DFT total energies of $g_{CeO_2}$, $g_{Ce}$ and $E_{O_2}$, the allowed range of the chemical potential of oxygen is $-5.01 \le \Delta\mu_O \le 0$ eV.[16] Analogous considerations can be obtained for water vapor, where the water-rich limit is restricted by considering water staying in the gas phase.[35] The upper limit of the relative chemical potential is $[\Delta\mu_{H_2O}]_{max} = -0.91$ eV, which is the value at the critical point. Hence, for water, we have $\Delta\mu_{H_2O} \le -0.91$ eV.[35]

Having established the ranges of the oxygen and water chemical potentials, we now turn to the determination of the surface phase diagram. To do this, for each stoichiometry investigated in this work, we consider only the most stable configuration. This is because, as we will see, different configurations corresponding to the same stoichiometry give rise to parallel planes in the ($\Delta\mu_O$, $\Delta\mu_{H_2O}$) domain. We label the most stable configuration of the water–ceria system $CeO_2 + H_2O$, and that of the water–ceria system with oxygen vacancies $CeO_2 + V_O + H_2O$, while $CeO_2 + V_O + OH + H$ indicates water dissociated on ceria with oxygen vacancies,

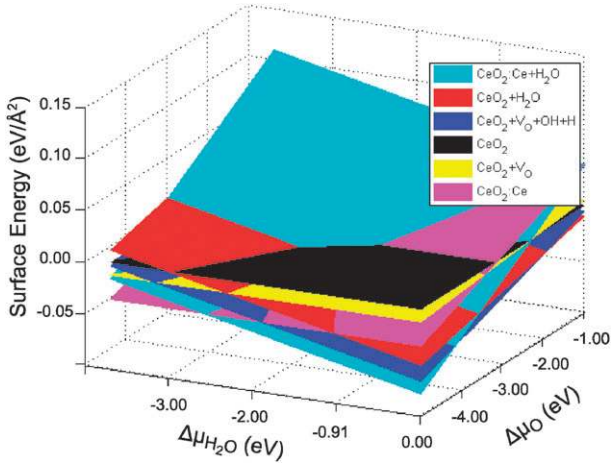


**Fig. 7** Surface free energies of the six most stable phases, as a function of $\Delta\mu_O$ and $\Delta\mu_{H_2O}$.

with the OH fragment filling the oxygen vacancy. The clean surface and the surface containing vacancies are labeled $CeO_2$ and $CeO_2 + V_O$ respectively, while the clean, highly-reduced ceria and water bonded on this reduced ceria surface are labeled $CeO_2$:Ce and $CeO_2$:Ce + $H_2O$, respectively.

Fig. 7 shows the dependence of the six surface energies as a function of $\Delta\mu_O$ and $\Delta\mu_{H_2O}$. Projecting the lowest surface free energies on the ($\Delta\mu_O$, $\Delta\mu_{H_2O}$) plane, we obtain the surface phase diagram shown in Fig. 8. We use eqn (6) and (7) to express the chemical potential of oxygen and water in terms of partial pressure at different temperatures. The temperature range of interest is between 300 K and 1200 K, while the typical experimental pressure range is between 1 atm and $10^{-14}$ atm (UHV). At low temperature (300 K), within the pressure range considered, the stable surfaces are $CeO_2$ + $H_2O$ and clean $CeO_2$, with the clean surface being the stable phase only under very low water partial pressures. At high temperature (1200 K), within the same pressure range, the structure containing oxygen vacancies, $CeO_2 + V_O$, and the clean $CeO_2$ are the stable phases. The highly-reduced ceria surface with and without adsorbed water, becomes stable for values of oxygen partial pressures too low to be taken into consideration for experimental conditions, even at high temperatures.

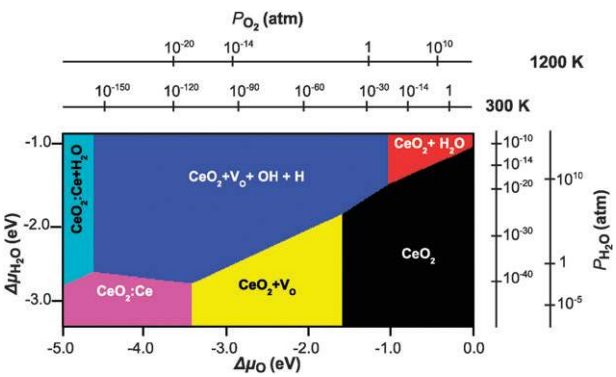


**Fig. 8** Surface phase diagram of stable structures of $CeO_2$(111) in equilibrium with a "humid environment", as a function of $\Delta\mu_O$ and $\Delta\mu_{H_2O}$ in the gas phase. The additional axes show the corresponding pressure scales at $T$ = 300 and 1200 K.

From an analysis of the phase diagram, there are two important phase transitions worth investigating. First, if we fix the pressure at 1 atm for both gases, we can move on the phase diagram by varying the temperature of both gas reservoirs. The resulting curve on the phase diagram in Fig. 8 would be an isobar line starting at 1200 K in the clean $CeO_2$ phase and crossing into the $CeO_2$ + $H_2O$ phase upon lowering the temperature. The transition temperature between these two phases is around 700 K. This indicates that, at this pressure, water adsorption on the clean surface is stable up to 700 K. Above this temperature water desorbs into the gas phase. To study how this transition temperature depends on the pressure of the two gases, we repeat the same analysis allowing the pressure of both gases to vary simultaneously in the range 1 to $10^{-14}$ atm. Fig. 9 shows the transition temperature as a function of pressure of the two gases. We can compare this result with experimental data obtained by temperature programmed desorption (TPD).[10] At a pressure of $\sim 10^{-10}$ atm, depending on the water coverage, these data show a peak in the TPD spectrum in the 200–320 K range. In particular, at a coverage of 0.20 ML, the desorption temperature is found to be 265 K. This value compares favorably with our estimated value of $\sim$350 K for similar conditions ($p_{O_2} = p_{H_2O} = 10^{-10}$ atm, $\Theta_{H_2O}$ = 0.25 ML). While estimating the error bars in the temperatures and pressures predicted using the *ab initio* atomistic thermodynamics approach is difficult, we note that such an estimate has been carried out for the O–Ag system,[42] leading to an estimated error of $\sim$100 K in the temperature and $\sim$3 orders of magnitude in the pressure.

Another phase transition worth investigating is what happens in water rich conditions (*i.e.* $\Delta\mu_{H_2O} = -0.91$ eV) as a function of $\Delta\mu_O$. We can see from Fig. 8 that by decreasing $\Delta\mu_O$ we go from a situation where water is bonded to the clean surface to a situation where water is dissociated at an oxygen vacancy. In light of the discussion presented in section IIIB, where we have shown that water dissociation at an oxygen vacancy is kinetically hindered by a large activation barrier, it

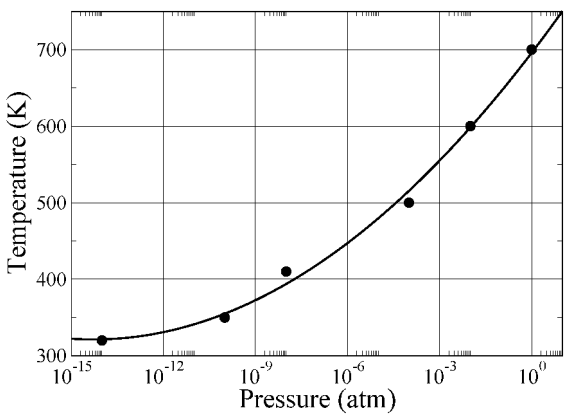


**Fig. 9** Temperature as a function of pressure above which the clean $CeO_2$(111) surface becomes more stable than the $CeO_2$(111) + $H_2O$ structure (in which water is adsorbed on the surface). The pressures of both gas reservoirs are assumed to be equal. Dots represent values of temperature extrapolated from experimental values of the chemical potential of water ($\Delta\mu_{H_2O}$), while the line is a polynomial interpolation of those values.

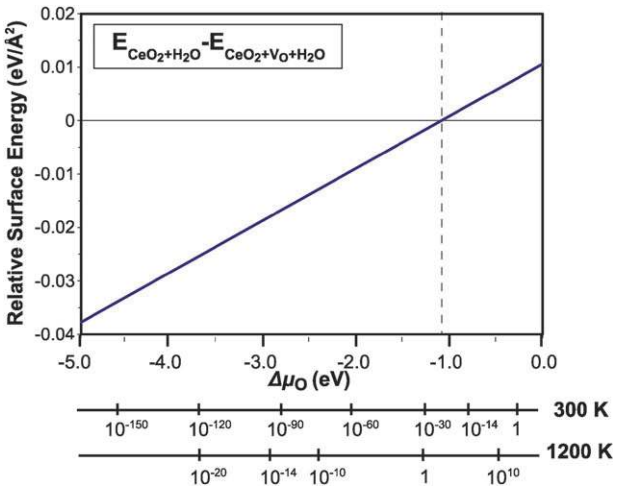


**Fig. 10** Difference in surface energy between water adsorbed on a clean surface and on a surface with oxygen vacancies, as a function of the oxygen chemical potential, $\Delta\mu_O$ for a given water-rich condition ($\Delta\mu_{H_2O} = -0.91$ eV). The additional axes show the corresponding pressure scales at $T = 300$ and 1200 K.

is also worth considering the metastable structure with water chemisorbed on an oxygen vacancy ($CeO_2 + V_O + H_2O$). This structure has the same stoichiometry and a very similar surface energy to the thermodynamically stable $CeO_2 + V_O + OH + H$, where water is dissociated into an OH fragment filling the oxygen vacancy and an H atom bonded to a surface oxygen. Given that the stoichiometry of the two structures is the same, and that the difference in surface energy is just 0.002 eV Å$^{-2}$, the surface phase diagram we would obtain by considering $CeO_2 + V_O + H_2O$ in place of $CeO_2 + V_O + OH + H$ would be indistinguishable from the one shown in Fig. 8. Starting from $CeO_2 + H_2O$, the phase transition induced by lowering the oxygen chemical potential can therefore be viewed as a reduction process in which the presence of water induces the creation of surface oxygen vacancies. We find that this phase transition takes place at $T \sim 450$ K under UHV conditions ($p_{O_2} = 10^{-12}$ atm) and at $T \sim 1000$ K at $p_{O_2} = 1$ atm. Fig. 10 shows this transition more clearly by plotting the surface free energy difference between the $CeO_2 + V_O + OH + H$ and $CeO_2 + H_2O$ structures as function of the oxygen chemical potential for a given water-rich condition (*i.e.* $\Delta\mu_{H_2O} = -0.91$ eV). Focusing on the UHV conditions, our results suggest that beyond 450 K the presence of water favors the creation of oxygen surface vacancies. This result is qualitatively consistent with recent experimental measurements where it has been shown that at 650 K, in UHV conditions, the presence of water increases the concentration of oxygen surface vacancies.[10]

## V. Vibrational contribution to the free energy

In this section we analyze the vibrational contribution to the total energy for the $CeO_2(111) + H_2O$ system in order to understand its effect on the stability of water adsorption. As we have seen in the previous section, at $p_{O_2} = 1$ atm, the region of stability of this phase is $T \leq 700$ K. Here we will determine how the explicit account of the (harmonic) vibrational contribution modifies this transition temperature. To address the stability of the adsorption structure, we compute the Gibbs free energy of adsorption, defined as

$$\Delta G = G^{\text{Surf–Mol}} - (G^{\text{Surf}} + G^{\text{Mol}}), \tag{14}$$

where $G^{\text{Surf–Mol}}$ is the Gibbs free energy of the surface–molecule system, while $G^{\text{Mol}}$ and $G^{\text{Surf}}$ are, respectively, the free Gibbs energy of the isolated molecule and the surface. The different contributions to the total Gibbs free energy of adsorption can be written explicitly as:

$$\Delta G = -E_b + \Delta F^{\text{vib}} + \Delta F^{\text{conf}} + \Delta(pV). \tag{15}$$

As shown in the previous section (see eqn (8)), $E_b$ represents the value of the binding energy of the adparticle to the surface per unit cell and $\Delta F^{\text{conf}}$ is the configurational entropy term. The order of magnitude of the $\Delta(pV)$ term is so small as it to be negligible.[37] In this study, we also neglect the configurational entropy contribution ($\Delta F^{\text{conf}}$) since we compare the relative stability of surfaces with different terminations (*i.e.* $CeO_2$, $CeO_2 + H_2O$). $\Delta F^{\text{vib}}$ (see eqn (16)) is the difference between the vibrational contribution to the free energy of the adsorption system minus the sum of the isolated surface and molecule in the gas phase:

$$\Delta F^{\text{vib}} = F^{\text{vib}}_{\text{Surf–Mol}} - (F^{\text{vib}}_{\text{Surf}} + F^{\text{vib}}_{\text{Mol}}). \tag{16}$$

Therefore we have:

$$\Delta G \simeq -E_b + \Delta F^{\text{vib}}. \tag{17}$$

The adsorption is favored when $\Delta G \simeq 0$. From eqn (17) it follows that the condition for stability of the adparticle is

$$\Delta F^{\text{vib}} \leq E_b. \tag{18}$$

To estimate the vibrational contribution to the free energy, we write, within the harmonic approximation, the contribution of a given vibrational mode at frequency $\omega_i$ as a function of $T$:[37]

$$F^{\text{vib}}(T, \omega_i) = \frac{1}{2}\hbar\omega_i + k_B T \ln(1 - e^{-\frac{\hbar\omega_i}{k_B T}}). \tag{19}$$

To calculate the total vibrational energy, for a certain $T$, we need to integrate eqn (19) with respect to the frequency spectrum of a particular system,

$$F^{\text{vib}}_{\alpha}(T) = \sum_{i=1}^{3N} F(T, \omega_i^{\alpha}), \tag{20}$$

where $\alpha$ is the label for the system considered (adsorption system, free molecule and clean surface) and $\omega_i^{\alpha}$ is the frequency spectrum of the system, $\alpha$. In the following we will consider only the vibrational contribution at the $\Gamma$ point, computed through the finite difference procedure, using a displacement of 0.01 $a_0$.

Considering first the frequency spectrum for the clean surface (see Fig. 11(b)), it can be seen that, compared to that of the bulk system (Fig. 11(a)), the spectrum is broader in the range 0 to 600 cm$^{-1}$, due to the formation of the surface. To obtain the vibrational contribution to the free energy of the water molecule, we use the experimental values of chemical potential, $\mu_{H_2O}$, which include both vibrational and rotational effects. Fig. 11(c) shows the frequency spectrum at the $\Gamma$ point

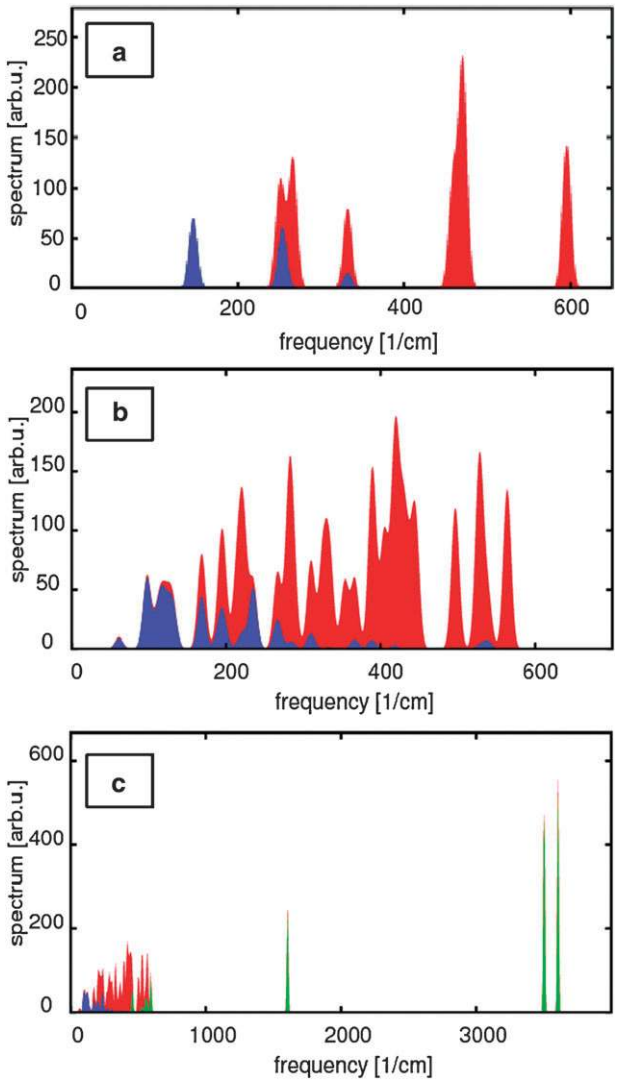


**Fig. 11** Phonon density-of-states of bulk $CeO_2$ (a), the $CeO_2$(111) surface (b) and the $CeO_2$(111) + $H_2O$ surface (c). The dark grey (red) areas represents the contribution of the cerium atoms, the grey (blue) areas represent the contribution of the oxygen atom and the light grey (green) areas at high frequency represent the contribution of the hydrogen atom.

for the surface–water molecule adsorption system. In this case, we obtain additional peaks due to the water–surface coupled modes and to the intrinsic modes of the water molecule.

In Fig. 12, we show the vibrational free energy of the two systems ($F^{vib}_{Surf–Mol}$ and $F^{vib}_{Surf} + F^{vib}_{Mol}$) as a function of temperature. The dashed line (blue) represents the vibrational energy for the water molecule adsorbed on the surface ($F^{vib}_{Surf-Mol}$). The continuous line (red) represents the sum of the contributions of the free molecule and the clean surface system ($F^{vib}_{Surf} + F^{vib}_{Mol}$), and the dot-dashed (green) line represents the difference in the vibrational contribution to the free energy due to the adsorption process: $\Delta F^{vib} = (F^{vib}_{Surf} + F^{vib}_{Mol}) - (F^{vib}_{Surf–Mol})$. According to eqn 18, the condition of stability of adsorption is $\Delta F^{vib} - E_b$. We recall that the calculated binding energy for the water molecule adsorbed on the $CeO_2$(111) surface is 0.49 eV. As shown in Fig. 12, the condition $\Delta F^{vib} \leq 0.49$ eV is satisfied

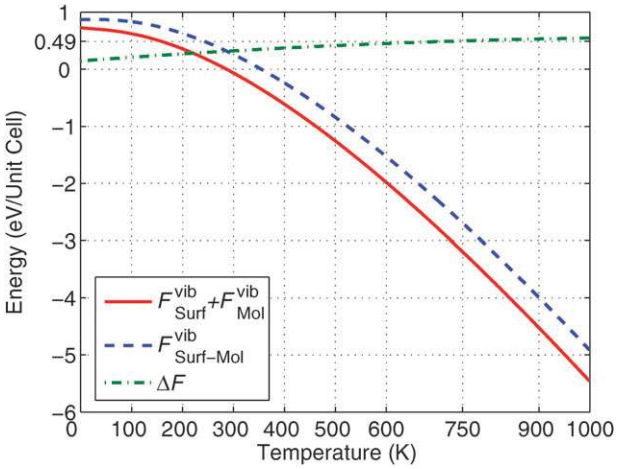


**Fig. 12** Vibrational energy contribution to the total energy as a function of temperature. The dashed (blue) line represents the vibrational energy for water adsorbed on the $CeO_2$(111) surface. The solid line (red) represents the vibrational energy of the free water molecule and the $CeO_2$(111) surface. The dot-dashed (green) line represents the difference between water adsorbed on the $CeO_2$(111) surface and the free water molecule and the $CeO_2$(111) surface.

for values of temperature $T \leq 750$ K. We can therefore conclude that, for temperature $T \leq 750$ K, the adsorption of the water on the $CeO_2$(111) surface is stable, while at higher temperatures water desorbs into the gas phase. Comparing the value of this transition temperature with the one obtained by neglecting the vibrational contributions (700 K), we see that the latter has the effect of stabilizing water adsorption on the surface. The overall effect, therefore, is to increase the transition temperature by 50 K. We stress, however, that this estimate was obtained within the harmonic approximation, which, at high temperature, might not be sufficient to fully describe the vibrational contributions to the free energy.

## VI. Summary and conclusions

In this work we performed DFT calculations to analyze the structure and energetics of water adsorption on the stoichiometric and reduced $CeO_2$(111) surface. On the stoichiometric surface, the most stable structure is the one in which water is adsorbed on Ce, forming two O–H bonds with the oxygen atoms of the surface. We find that surface oxygen vacancies increase the binding energy of water molecules (*i.e.* making them more stable). Also, the vacancy formation energy is lower when water is adsorbed on the surface, compared to the case when a vacancy is created on the clean surface. Our results show that water does not dissociate on the clean surface, while on the surface with oxygen vacancies this process becomes thermodynamically favorable. However, from analysis of the activation barrier of water dissociation on the reduced surface, which we estimate to be 2.35 eV, this process seems unlikely except at very high temperatures, consistent with experimental evidence.

There are, however, some discrepancies in the calculated binding energies when we compare some of our results with other theoretical works. Part of these discrepancies can be

 

attributed to the difficulty in locating the most stable among several local minima in the adsorption configurations of water on ceria. We have also shown that different choices of surface unit cell induce different lateral interactions among the adsorbates which, in the case of atomic hydrogen, lead to a strong dependence of the binding energy on the coverage.

By employing the *ab initio* constrained thermodynamics approach, we constructed the surface phase diagram and studied the phase transition between water physisorbed on the stoichiometric surface and water chemisorbed on the reduced surface (with oxygen vacancies). The phase diagram shows that, under UHV conditions, and beyond a temperature of 450 K, the reduced surface with adsorbed water becomes more favorable than the clean surface with adsorbed water. Our results are consistent with experiments performed in UHV at 650 K which show that the presence of water increases the surface oxygen vacancies concentration. We also studied the water desorption process on the stoichiometric surface. We extrapolated the water desorption temperature from the clean surface (700 K), considering the pressure of both gases, water and oxygen, to be fixed at 1 atm. By varying the partial pressure of both gases simultaneously, we calculated the desorption temperature from the clean surface as a function of pressure. Experimental data show that for a coverage of 0.20 ML, at pressure $p = 10^{-10}$ atm, water desorbs from the clean surface at $T = 265$ K. In our case, for a coverage of 0.25 ML, and the same value of pressure, the desorption temperature is 350 K. We also analyzed the vibrational contribution to the free energy at the $\Gamma$ point for water adsorbed on the clean surface. Including this term, the resulting desorption temperature at $p = 1$ atm is 750 K, *i.e.* an increase of 50 K.

## Acknowledgements

The authors gratefully acknowledge support from the Australian Research Council (ARC), the Australian Partnership for Advanced Computing (APAC), National Supercomputing Facility and the Australian Center for Advanced Computing and Communication (ac3).

## References

1 L. Saraf, C. M. Wang, V. Shutthanandan, Y. Zhang, O. Marina, D. Baer, S. Thevuthasan, P. Nachimuthu and D. Lindle, *J. Mater. Res.*, 2005, **20**, 1295.
2 S. Kim and J. Mayer, *J. Eur. Ceram. Soc.*, 2004, **24**, 1919.
3 A. Trovarelli, *Catal. Sci. Series*, 2002, **2**, 407.
4 A. Trovarelli, *Catal. Rev.*, 1996, **38**, 439.
5 M. S. Dresselhaus and I. L. Thomas, *Nature*, 2001, **414**, 332.
6 V. Esposito and E. Traversa, *J. Am. Ceram. Soc.*, 2008, **91**(4), 1037.
7 S. Kumar and P. Shelling, *J. Chem. Phys.*, 2006, **125**, 204704.
8 N. Laosiripojana, D. Chadwick and S. Assabumrungrat, *Chem. Eng. J.*, 2008, **138**, 264.
9 G. Avgouropoulosa and T. Ioannides, *Appl. Catal., B*, 2006, **67**, 1.
10 M. A. Henderson, C. L. Perkins, M. H. Engelhard, S. Thevuthasan and C. H. F. Peden, *Surf. Sci.*, 2003, **526**, 1.
11 M. B. Watkins, A. S. Foster and A. L. Shluger, *J. Phys. Chem. C*, 2007, **111**, 15337.
12 H. Chen, Y. Choi, M. Liu and M. C. Lin, *ChemPhysChem*, 2007, **8**, 849.
13 U. Berner, K. Schierbaum, G. Hones, P. Wincott, S. Haq and G. Thornton, *Surf. Sci.*, 2000, **467**, 201.
14 L. Kundakovic, D. Mullins and S. Overbury, *Surf. Sci.*, 2000, **457**, 51.
15 C. Pedeste, N. Cant and D. Trimm, *Catal. Lett.*, 1993, **18**, 305.
16 M. Fronzi, A. Soon, B. Delley, E. Traversa and C. Stampfl, *J. Chem. Phys.*, 2008, DOI: 10.1063/1.3191784.
17 M. V. Ganduglia-Pirovano, J. L. F. Da Silva and J. Sauer, *Phys. Rev. Lett.*, 2009, **102**, 026101.
18 H.-Y. Li, H.-F. Wang, X.-Q. Gong, Y.-L. Guo, Y. Guo, G. Lu and P. Hu, *Phys. Rev. B: Condens. Matter Mater. Phys.*, 2009, **79**, 1.
19 S. Torbugge, M. Reichling, A. Ishiyama, S. Morita and O. Custance, *Phys. Rev. Lett.*, 2007, **99**, 056101.
20 T. Halgren and W. Lipscomb, *Chem. Phys. Lett.*, 1977, **49**, 225.
21 Z. Yang, T. K. Woo, M. Baudin and K. Hermansson, *J. Chem. Phys.*, 2004, **120**, 16.
22 S. Fabris, S. De Gironcoli, S. Baroni, S. Vicario and G. Balducci, *J. Phys. Chem. B*, 2005, **72**, 237102.
23 S. Fabris, S. Vicario, G. Balducci, S. De Gironcoli and S. Baroni, *J. Phys. Chem. B*, 2005, **109**, 22860.
24 M. Nolan and G. W. Watson, *J. Phys. Chem. B*, 2006, **110**, 16600.
25 M. Huang and S. Fabris, *J. Phys. Chem. C*, 2008, **112**, 8643.
26 J. L. F. Da Silva, M. V. Ganduglia-Pirovano and J. Sauer, *Phys. Rev. B: Condens. Matter Mater. Phys.*, 2007, **75**, 045121.
27 M. Cococcioni and S. De Gironcoli, *Phys. Rev. B: Condens. Matter Mater. Phys.*, 2005, **71**, 035105.
28 S. Fabris, S. De Gironcoli, S. Baroni, G. Vicario and G. Balducci, *Phys. Rev. B: Condens. Matter Mater. Phys.*, 2005, **71**, 041102.
29 Y. Jiang, J. B. Adams and M. van Schilfgaarde, *J. Chem. Phys.*, 2005, **123**, 064701.
30 Y. M. Chiang, E. B. Lavik and D. A. Bloom, *Nanostruct. Mater.*, 1997, **9**, 663.
31 J. P. Perdew, K. Burke and M. Ernzerhof, *Phys. Rev. Lett.*, 1996, **77**, 3865.
32 B. Delley, *J. Chem. Phys.*, 1990, **92**, 508.
33 B. Delley, *J. Chem. Phys.*, 2000, **113**, 7756.
34 K. Reuter and M. Scheffler, *Phys. Rev. B: Condens. Matter Mater. Phys.*, 2003, **68**, 045407.
35 Q. Sun, K. Reuter and M. Sheffler, *Phys. Rev. B: Condens. Matter Mater. Phys.*, 2003, **67**, 205424.
36 X. C. Wang and M. Scheffler, *Phys. Rev. Lett.*, 2000, **84**, 3650.
37 K. Reuter and M. Scheffler, *Phys. Rev. B: Condens. Matter Mater. Phys.*, 2001, **65**, 035406.
38 M. W. Chase, *NIST-JANAF Thermochemical Tables*, American Institute of Physics, Woodbury, N.Y., 1998, vol. 2nd edn.
39 S. Gritschneder and M. Reichling, *Nanotechnology*, 2007, **18**, 044024.
40 S. Gritschneder, Y. Iwasawa and M. Reichling, *Nanotechnology*, 2007, **18**, 044025.
41 M. Prin, M. Pijolat, M. Soustelle and O. Touret, *Thermochim. Acta*, 1991, **186**, 273.
42 W. X. Li, C. Stampfl and M. Scheffler, *Phys. Rev. B: Condens. Matter Mater. Phys.*, 2003, **67**, 045408.